



Aqueous microdroplets enable abiotic synthesis and chain extension of unique peptide isomers from free amino acids

Dylan T. Holden^a, Nicolás M. Morato^a, and R. Graham Cooks^{a,1}

Contributed by R. Graham Cooks; received July 22, 2022; accepted August 27, 2022; reviewed by Veronica Bierbaum and Evan Williams

Amide bond formation, the essential condensation reaction underlying peptide synthesis, is hindered in aqueous systems by the thermodynamic constraints associated with dehydration. This represents a key difficulty for the widely held view that prebiotic chemical evolution leading to the formation of the first biomolecules occurred in an oceanic environment. Recent evidence for the acceleration of chemical reactions at droplet interfaces led us to explore aqueous amino acid droplet chemistry. We report the formation of dipeptide isomer ions from free glycine or L-alanine at the air–water interface of aqueous microdroplets emanating from a single spray source (with or without applied potential) during their flight toward the inlet of a mass spectrometer. The proposed isomeric dipeptide ion is an oxazolidinone that takes fully covalent and ion-neutral complex forms. This structure is consistent with observed fragmentation patterns and its conversion to authentic dipeptide ions upon gentle collisions and for its formation from authentic dipeptides at ultra-low concentrations. It also rationalizes the results of droplet fusion experiments that show that the dipeptide isomer facilitates additional amide bond formation events, yielding authentic tri- through hexapeptides. We propose that the interface of aqueous microdroplets serves as a drying surface that shifts the equilibrium between free amino acids in favor of dehydration via stabilization of the dipeptide isomers. These findings offer a possible solution to the water paradox of biopolymer synthesis in prebiotic chemistry.

mass spectrometry | prebiotic chemistry | air–water interface | dipeptide | origin of life

Many theories on the chemical origin of life presuppose the formation of rudimentary biomolecules (e.g., simple nucleotides, peptides, lipids) from less complex abiotic precursors through low-probability interactions in an oceanic environment (1, 2). A suite of geochemical scenarios has been proposed to address the entropic difficulties associated with chemical synthesis starting with low concentration precursors; they include hydrothermal vents (3–5), drying beaches (6), hot springs (7), meteorites or icy bodies (8–11), atmospheric aerosols (12, 13), and mineral surfaces (14–20).

In addition to these challenges, the formation of biopolymers (viz. oligonucleotides, proteins, polysaccharides) necessary to create and sustain living systems requires condensation (i.e., water loss) reactions between monomers, which chemical equilibrium makes decidedly unfavorable in water. The ubiquity of both water and condensation reactions in the prebiotic formation of biopolymers (as well as the necessity of water for life processes), the so-called water paradox (21), suggests highly specific conditions and/or the presence of robust and generalizable processes capable of facilitating such chemistry prior to the appearance of proto-enzyme catalysts. This point has been addressed through a variety of approaches which seek to explain the global or localized removal of water from a system to favor condensation (16–20, 22–27).

Of particular interest is the observation that the air–water interface of monolayers and thin films (28–31), inverted micelle aerosols (12), Leidenfrost droplets (32–36), and charged or neutral microdroplets (37–46) all reveal vastly different chemical kinetics compared to bulk, with rate constants increased by up to six orders of magnitude (47, 48). This interfacial acceleration phenomenon has been reported for prebiotically relevant reactions including condensation (12, 21, 29, 49–53), redox (54, 55), nucleophilic addition (41, 43), and ultraviolet-initiated photopolymerization reactions (56). The observed rate constant is associated with high surface-to-volume ratios, and it has been attributed to the partial solvation of species at the interface (47, 48, 57, 58) along with the high electric field at the air–solvent interface (55, 59–61). Other factors such as high degrees of mass transfer and mixing (62–64), ordered molecular orientation (38, 65), extremes in surface pH (41, 43, 66, 67), and increased reagent confinement (63, 68) might also contribute to the observed reaction acceleration in special cases. This topic and its applications have been reviewed several times (47, 57, 69).

Multiple studies have described dehydration reactions occurring at the air–water interface of aqueous microdroplets (25, 29, 49, 51, 52, 70). Others have reported that

Significance

Enzymes are needed for protein synthesis *in vivo* because dehydration in water to give amide bonds is highly unfavorable. However, conditions that permit the abiotic production of peptides in aqueous environments are a prerequisite for accepted origin of life chemistry. Here, we report a unique reactivity of free amino acids at the air–water interface of micron-sized water droplets that leads to the formation of peptide isomers on the millisecond timescale. Akin to many plausible prebiotic chemical systems (e.g., sea spray), this reaction is performed under ambient conditions and does not require additional reagents, acid, catalysts, or radiation. These findings exemplify the uniqueness of interfacial physicochemical processes and add support to the potential role of confined-volume systems in abiogenesis.

Author affiliations: ^aDepartment of Chemistry, Purdue University, West Lafayette, IN 47907

Author contributions: D.T.H., N.M.M., and R.G.C. designed research; D.T.H. and N.M.M. performed research; D.T.H., N.M.M., and R.G.C. analyzed data; and D.T.H., N.M.M., and R.G.C. wrote the paper.

Reviewers: V.B., University of Colorado Boulder; and E.W., University of California at Berkeley.

The authors declare no competing interest.

Copyright © 2022 the Author(s). Published by PNAS. This article is distributed under [Creative Commons Attribution-NonCommercial-NoDerivatives License 4.0 \(CC BY-NC-ND\)](https://creativecommons.org/licenses/by-nc-nd/4.0/).

See [online](https://www.pnas.org/lookup/suppl/doi:10.1073/pnas.2212642119/-/DCSupplemental) for related content such as Commentaries.

¹To whom correspondence may be addressed. Email: cooks@purdue.edu.

This article contains supporting information online at <http://www.pnas.org/lookup/suppl/doi:10.1073/pnas.2212642119/-/DCSupplemental>.

Published October 3, 2022.

the free energy of some endothermic reactions in bulk solution are negative when reagents are at the surface of the droplet, leading to spontaneous conversion (49, 51, 71). Note, however, that all of these prior studies of prebiotic microdroplet reactions utilized additional means to adjust equilibrium in favor of the condensation processes; these means included the use of amino acid esters (29), stabilization using divalent metal cations (29, 52), and/or addition of high concentrations of phosphoric acid (49, 51, 52, 70). Here, we take advantage of the unique characteristics of aqueous microdroplets containing only free amino acids, a likely common prebiotic system akin to atmospheric aerosols or sea spray, to demonstrate facile amide bond formation, generating unique peptide isomers on the millisecond timescale. These droplet-synthesized peptide isomers possess increased reactivity with other amino acids compared to their authentic dipeptide counterparts, as demonstrated by droplet–fusion reactions. This reactivity provides a plausible route for the formation of the first biopolymers in aqueous environments.

Results and Discussion

Gly and Alanine Dipeptide Formation in Microdroplets Monitored by MS. Aqueous droplets containing only glycine (Gly) or L-alanine (Ala) were generated by nano-electrospray ionization (nESI; Fig. 1C), and products in the spray were monitored by mass spectrometry (MS) (*SI Appendix* for experimental details). The dipeptides glycylglycine (GlyGly) and L-alanyl-L-alanine

(AlaAla), formed by the reaction of the amino acids (Fig. 1A and B) during the flight of the microdroplets to the inlet of the mass spectrometer, were sought as protonated or deprotonated species in the full scan mass spectra (Fig. 1E–H; *cf* spectra of pure authentic dipeptides shown in *SI Appendix*, Fig. S1). Electrospray ionization (ESI)-MS is an established method for bulk reaction monitoring; it can generate larger droplets (lower surface-to-volume ratio) than nESI with negligible reaction acceleration effects. ESI, therefore, was used to examine the potential presence of trace dipeptides through reactions of amino acids. No peaks at the m/z values corresponding to the presumptive dipeptides could be detected in bulk (*SI Appendix*, Fig. S2), even after a 2-h incubation of the amino acid solutions at room temperature.

To investigate further the nature of the observed amino acid reactivity in nESI droplets, the effect of both spray distance (i.e., distance between the nESI emitter and the inlet of the mass spectrometer; Fig. 1C) and voltage (using a pneumatically assisted variant of ESI; Fig. 1D) was investigated. The application of an external potential was found to be unnecessary to form presumptive dipeptides (Fig. 1J). This result demonstrates the inherent reactivity at the air–water interface of microdroplets. Similarly, Fig. 1I shows an increase in the conversion to presumptive dipeptides (*SI Appendix*, Eq. S1) with spray distance (*SI Appendix*, Fig. S3 for spectra), indicating a droplet-associated reaction. The observed increase in product is likely due to a combination of longer reaction time at the air–water interface

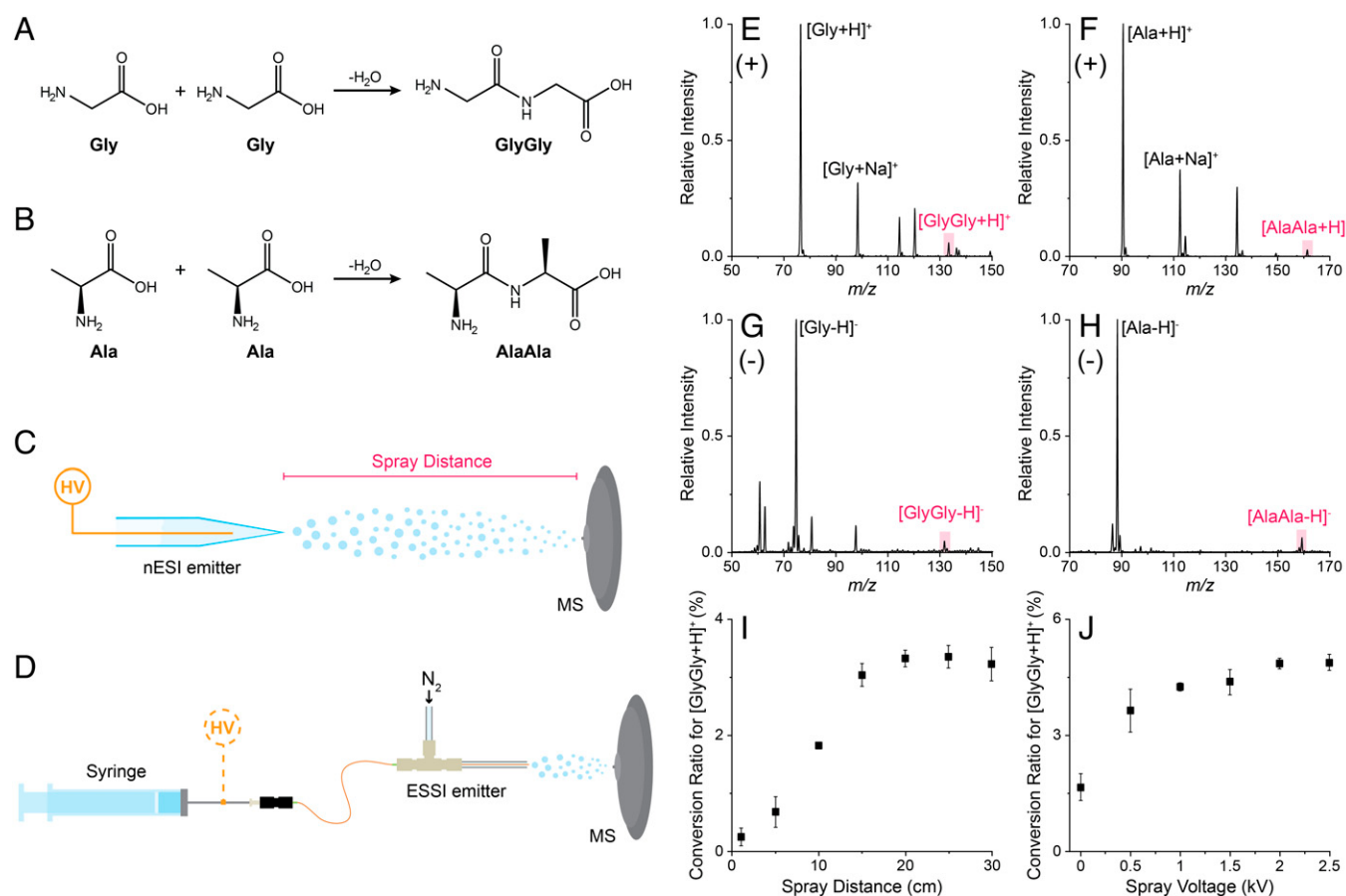
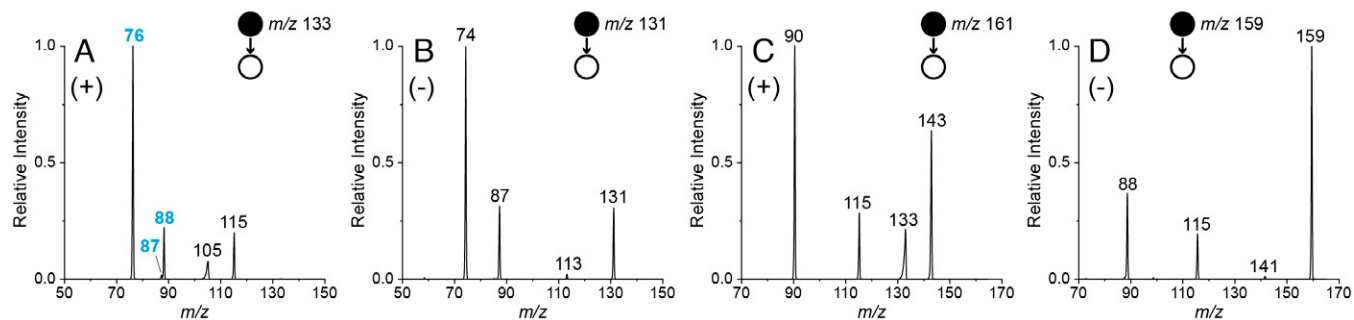


Fig. 1. Reactions, experimental setups, and spray parameter effects associated with the spontaneous generation of putative dipeptides from free amino acids in aqueous microdroplets. *A* and *B* show condensation reactions yielding GlyGly and AlaAla from free Gly and Ala, respectively. *C* and *D* illustrate the experimental arrangements including high voltage (HV) utilized to generate microdroplets in nESI (*C*) and ESSI (*D*). *E* through *H* show the full-scan nESI spectra for aqueous solutions (5 mM) of Gly (*E* and *G*) and Ala (*F* and *H*) in both the positive (*E* and *F*) and negative ion (*G* and *H*) modes. The observed presumptive dipeptide peaks are labeled in all cases. *I* and *J* summarize the effects of the spray distance and voltage, respectively, on the positive ion conversion ratio to GlyGly. Conversion ratios were calculated using the average of 50 scans in triplicate. Error bars indicate SDs.

MS/MS Spectra of Standard Reference Dipeptides:



MS/MS Spectra of Microdroplet-Generated Products:

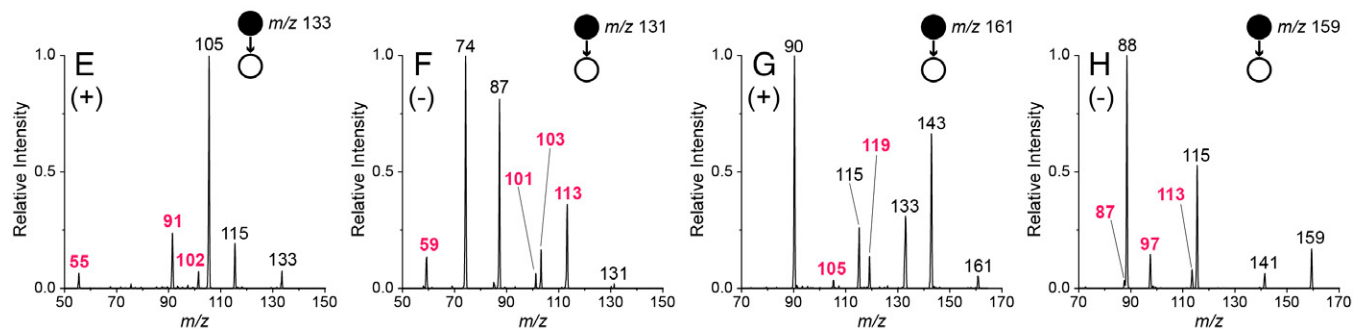


Fig. 2. Comparison of nESI-MS/MS spectra obtained for the standard (*Top Row, A–D*) and droplet-synthesized (*Bottom Row, E–H*) dipeptides. Results are shown for both protonated (*A* and *E*) and deprotonated (*B* and *F*) GlyGly, as well as protonated (*C* and *G*) and deprotonated (*D* and *H*) AlaAla. Droplet-synthesized spectra (*Bottom Row*) were obtained by spraying pure amino acid solutions in water, whereas standard spectra (*Top Row*) were acquired from aqueous solutions of commercial dipeptide standards. Annotated in blue are the unique peaks in the spectra of the standard compounds, while the unique reaction product fragments are in pink.

and continued droplet fission events (72), which occur spontaneously but are enhanced by the application of a potential.

Dipeptide Isomers Revealed by MS/MS. Tandem MS (MS/MS) analysis of the droplet-synthesized products was performed to verify their identity. Ions of interest (both polarities) were mass selected and subjected to ion trap collision-induced dissociation (IT-CID). Protonated authentic GlyGly, when fragmented, gave the product ions reported in common MS/MS databases (Fig. 2*A*) (73). In contrast, several unique peaks were present in the product ion spectrum of the droplet-synthesized GlyGly product, while some of the fragments expected for the authentic

compound were not observed (Fig. 2*E*). Similarly, protonated authentic AlaAla fragmented as expected (73) (Fig. 2*C*), while the protonated droplet-synthesized AlaAla showed additional peaks (Fig. 2*G*). Similar comparisons were carried out for authentic and droplet-synthesized compounds for deprotonated GlyGly (Fig. 2*B* and *F*) and AlaAla (Fig. 2*D* and *H*).

High-resolution MS (HRMS) was used to determine the exact mass and predict the chemical formula of the microdroplet-generated species. In all cases, the values found match those of the authentic dipeptides, confirming the microdroplet-mediated formation of dipeptide isomers. IT-CID followed by HRMS analysis was used to identify the diagnostic product ions for the

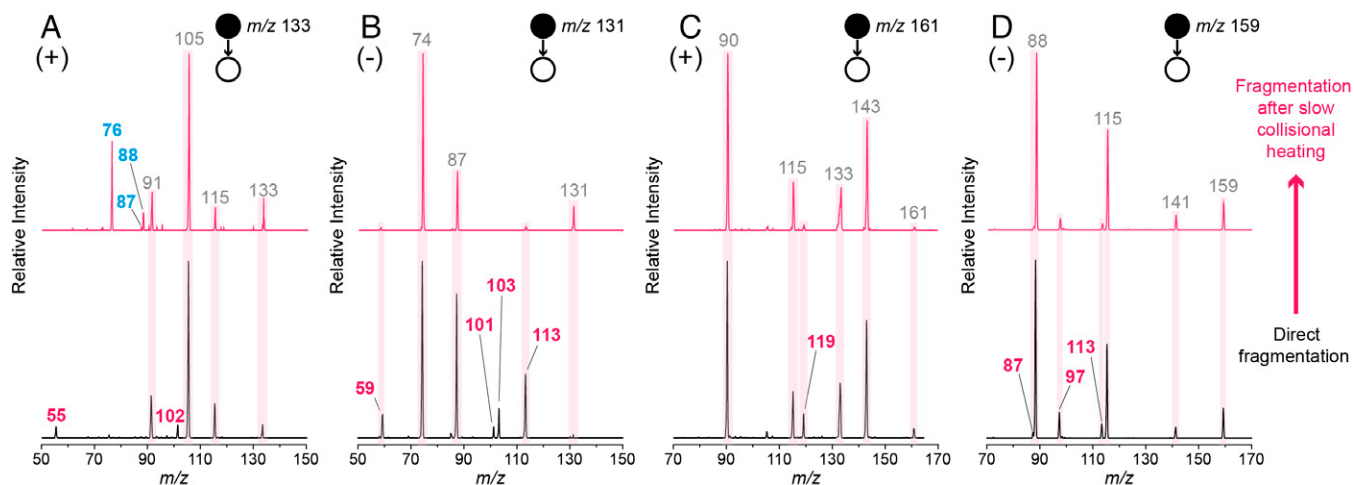


Fig. 3. Differences in the MS/MS spectra of the isomeric dipeptide species before (*Bottom*) and after (*Top*) collisional heating (30 s at CE < fragmentation threshold). Results for both the protonated (*A*) and deprotonated (*B*) GlyGly isomer, as well as the protonated (*C*) and deprotonated (*D*) AlaAla isomer, are shown. Annotated in blue are the unique peaks present in the spectra of the isomeric compound prior to heating, which disappear partially or completely after collisional heating. Annotated in pink are the unique standard dipeptide fragments which appear in the isomer spectra after collisional heating.

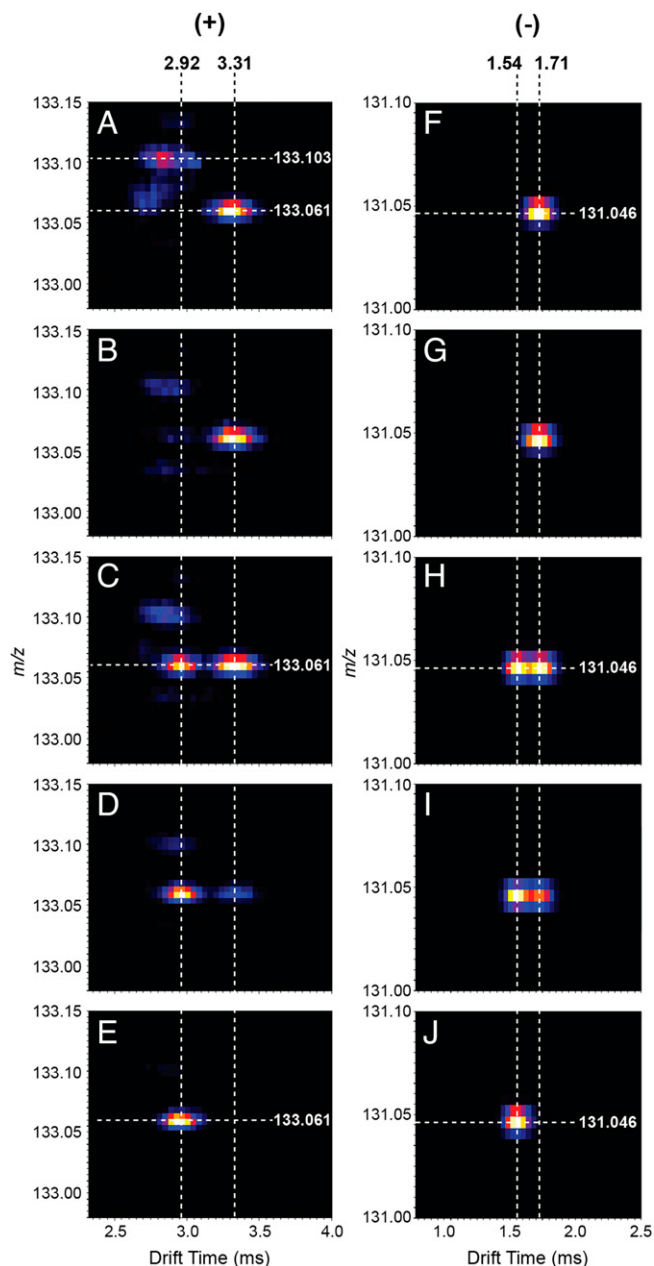


Fig. 4. Two-dimensional plots of m/z vs. drift time of aqueous solutions with different proportions of Gly and GlyGly (concentration of Gly increases from *Top to Bottom*). Results for both the positive (*Left*) and the negative (*Right*) ion mode are included. The solutions analyzed were as follows: 100% GlyGly (A and F), 1:125 GlyGly-Gly (B and G), 1:375 GlyGly-Gly (C and H), 1:500 GlyGly-Gly (D and I), and 100% Gly (E and J). Average drift times of the protonated isomeric and standard species were determined as 2.92 ± 0.02 ms and 3.31 ± 0.01 ms, respectively. For the deprotonated species, the average drift times were 1.54 ± 0.01 ms (isomer) and 1.71 ± 0.02 ms (authentic). Note that IMS conditions are substantially different for the two polarities as they were optimized separately to maximize resolution in drift time separation.

protonated and deprotonated authentic and isomeric dipeptides (*SI Appendix*, Table S1).

In-Trap Isomerization of Dipeptides by Collisional Heating. To compare the stability of the authentic and droplet-synthesized dipeptides, the relationship between the relative abundance of each product ion as a function of collision energy (CE) was visualized using breakdown curves (*SI Appendix*, Fig. S4). In all four cases (i.e., for protonated and deprotonated GlyGly and AlaAla), it was observed that the isomeric dipeptides fragmented more readily than the corresponding authentic compounds. It should

be noted, however, that quantitative thermochemical measurements cannot be made from these breakdown curves due to the relatively slow ion activation process and the limited capabilities to control ion kinetic energy in IT-CID (74).

Isomerization of the droplet-synthesized dipeptides was observed during collisional heating at CE values just below the fragmentation thresholds. Slow collisional heating is a well-known method of imparting internal energy to mass-selected ions via numerous low-energy collisions with the inert bath gas. In some cases, this can lead to the isomerization of the isolated species (75–77). With heating, the fragmentation profiles of the protonated and deprotonated droplet-synthesized dipeptides increasingly matched those of the authentic dipeptides (Fig. 3). By contrast, no significant changes in the spectra of the protonated or deprotonated authentic dipeptides were observed following collisional heating (*SI Appendix*, Fig. S5). The observed slow heating-induced conversion suggests the presence of low-energy pathways leading from the dipeptide isomer ions to the authentic dipeptide structures, as discussed further below.

Separation of Dipeptide Isomers by IMS. Ion mobility spectrometry (IMS) coupled with MS was used to evaluate structural differences between the authentic dipeptides and the droplet-generated isomers using a series of aqueous solutions with various Gly:GlyGly ratios (for details, *SI Appendix*). When a solution of pure authentic GlyGly was sprayed and analyzed in positive ion mode, the two-dimensional plot of drift time vs. m/z revealed a high intensity feature at a drift time of ca. 3.3 ms and an m/z value of 133.061 (Fig. 4A), corresponding to protonated GlyGly. As the proportion of Gly was increased, an additional feature at the same m/z value, attributed to the microdroplet-synthesized dipeptide isomer, appeared and increased in intensity (Fig. 4B–D). This ion showed a lower drift time (ca. 2.9 ms) than authentic protonated GlyGly. Using Gly in 500 \times excess relative to authentic GlyGly, the signal for this unique species became dominant (Fig. 4D), and it is the only feature present when pure Gly is sprayed (Fig. 4E). The lower drift time of the GlyGly dipeptide isomer suggests a more compact structure compared to the authentic GlyGly. A similar trend can be observed when the same experiment is performed in the negative ion mode (Fig. 4F–J). The drift times for the positive ions were remeasured as collision cross-sections after calibration of the IMS instrument, and the result for authentic GlyGly was $126.7 \pm 0.1 \text{ \AA}^2$, while the isomeric dipeptide was $120.8 \pm 0.2 \text{ \AA}^2$. These findings provide strong evidence for the presence of a more compact microdroplet-synthesized isomeric species compared to the authentic dipeptide ions.

Peptide Extension Reactions Using Droplet Fusion. To probe the reactivity of the microdroplet-synthesized isomers, we utilized droplet fusion (Fig. 5A), an experiment that simulates water droplet collisions in the atmosphere or in sea sprays. This technique has been implemented previously to study acid-induced unfolding and hydrogen–deuterium exchange of proteins in microdroplets (78), as well as demetallation reactions (37). Experimental details are included in the *SI Appendix*.

Upon the collision of two Gly spray plumes (nESI, ± 2 kV spray voltage), the mass spectrum revealed the formation of protonated triglycine (Gly₃) and tetraglycine (Gly₄) (Fig. 5C). The IT-CID MS/MS fragmentation profiles of these ions agree with the corresponding authentic spectra (*SI Appendix*, Fig. S6, cf. A and B, C, and D), suggesting that the isomeric dipeptides

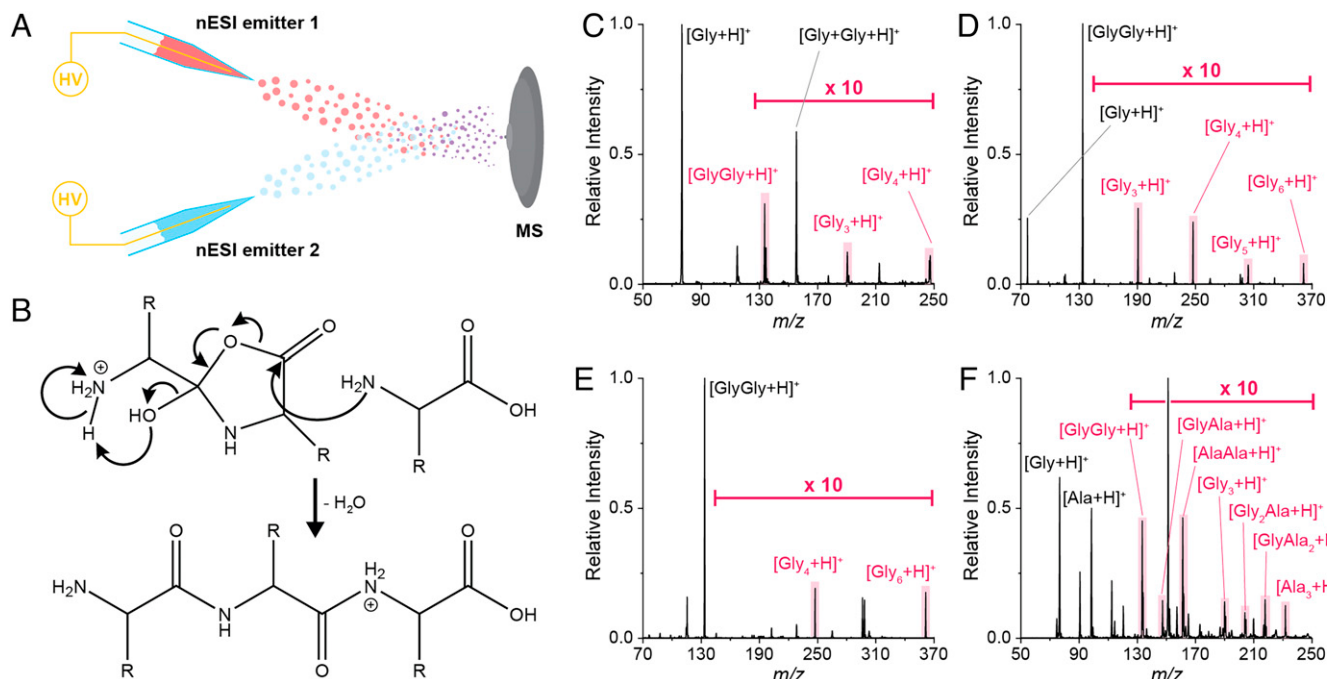


Fig. 5. Droplet-fusion experiment (A), proposed isomer chain extension reaction from structure 1 (B), and resulting full-scan mass spectra (C–F). When aqueous solutions of Gly are sprayed from both nESI emitters (C), di-, tri-, and tetrapeptides are observed in the mass spectrum. Similarly, if both emitters are used to spray GlyGly (E), only tetra and hexapeptides are obtained, as would be expected. When spraying Gly from one nESI emitter and GlyGly from the other (D), a range of oligomers up to hexapeptide species is detected. Finally, when spraying mixtures of Gly and Ala from both emitters, all possible homo- and heterostructures are represented in the m/z values observed up to tripeptides (F). The generated peptide species are highlighted in all cases. During droplet fusion, the unique microdroplet-synthesized dipeptide isomers (either oxalidinone as shown or as an ion-neutral complex) serve as chain extension species that undergo further condensation reactions with other amino acids or peptides to yield authentic higher-order peptides (B).

are forming authentic higher-order peptides. GlyGly spray plumes generated protonated Gly₄ and hexaglycine (Gly₆) (Fig. 5D), whereas colliding a spray of Gly and a spray of GlyGly produced all peptides from Gly₃ to Gly₆ (Fig. 5E). As expected, there is a greater abundance of Gly₃ and Gly₄ compared to pentaglycine (Gly₅) and Gly₆, which require at least two reaction events. Note that a Gly and GlyGly mixture, sprayed from a single nESI capillary, generates a trace amount of Gly₃, although there are no higher-order peptide products (SI Appendix, Fig. S7). Similar results are obtained in the negative ion mode (SI Appendix, Fig. S8).

Using Ala in each emitter, dipeptide isomers as well as tri- (Ala₃) and tetra-L-alanine (Ala₄) (SI Appendix, Fig. S9) are obtained. As with Gly, the fragmentation profiles of these larger peptides match those of the authentic compounds (SI Appendix, Fig. S10). Finally, spraying a mixture of Gly and Ala from both emitters yielded protonated GlyGly and AlaAla isomers, Gly₃ and Ala₃, as well as Gly₂Ala and GlyAla₂ heteropeptides (Fig. 5F; SI Appendix, Fig. S11 for MS/MS spectra). Notably, based on the MS/MS spectra, the droplet fusion reaction between Gly and Ala seems to favor the formation of GlyAla over AlaGly (*cf* SI Appendix, Fig. S11 A–C). No GlyAla or AlaGly dipeptides were formed from a single emitter nESI spray of the mixture.

There are several factors that may contribute to the success of these droplet fusion reactions. The increased number of microdroplet collisions should enable a greater number of fission events after the droplets have collided, resulting in smaller droplets with greater surface-to-volume ratios. Increased collisions could also provide enough turbulent force to perturb the droplet surface (without fission) thereby enabling a greater degree of solvent evaporation, which is typically negligible during the flight time of aqueous microdroplets (72, 78). Other phenomena involving the interactions of the strong interfacial

electric fields upon droplet collision may also contribute to the observed reactivity (79). Importantly, these results suggest an increased and unique reactivity of the synthesized isomeric dipeptides compared to their standard counterparts, a feature that may be significant with respect to peptide formation and extension in prebiotic environments.

Insights into Mechanism. The observed dipeptide isomers could be generated through two pathways, as follows: 1) accelerated formation of the authentic dipeptide product at the air–droplet interface where it then isomerizes and/or 2) a unique mechanism of amide bond formation between free amino acids at the droplet surface that directly forms the isomeric product. The results of the MS/MS analysis and collisional heating of the authentic dipeptides (SI Appendix, Fig. S5) suggest that they are incapable of isomerizing to any meaningful extent, favoring the second, more direct, pathway. However, these results correspond to the analysis of the authentic species at micromolar to millimolar concentrations, which disproportionately represent the molecules present in the bulk portion of the microdroplets rather than those at the surface.

Therefore, to assess differences in the behavior of the authentic dipeptide when at the droplet surface vs. bulk, we performed identical nESI-MS/MS experiments as described above, albeit using 10 pM aqueous solutions of authentic GlyGly and AlaAla, expecting that the significantly lower concentration would allow for interrogation of a larger proportion of the molecules at the droplet surface. Under these conditions, the fragmentation profiles of the authentic dipeptides represent a combination of those from the corresponding authentic and isomeric species (SI Appendix, Fig. S12), suggesting that the detected isomeric dipeptide can be formed from the authentic dipeptide at the air–droplet interface. These results imply that the microdroplet reaction of amino acids may be producing the

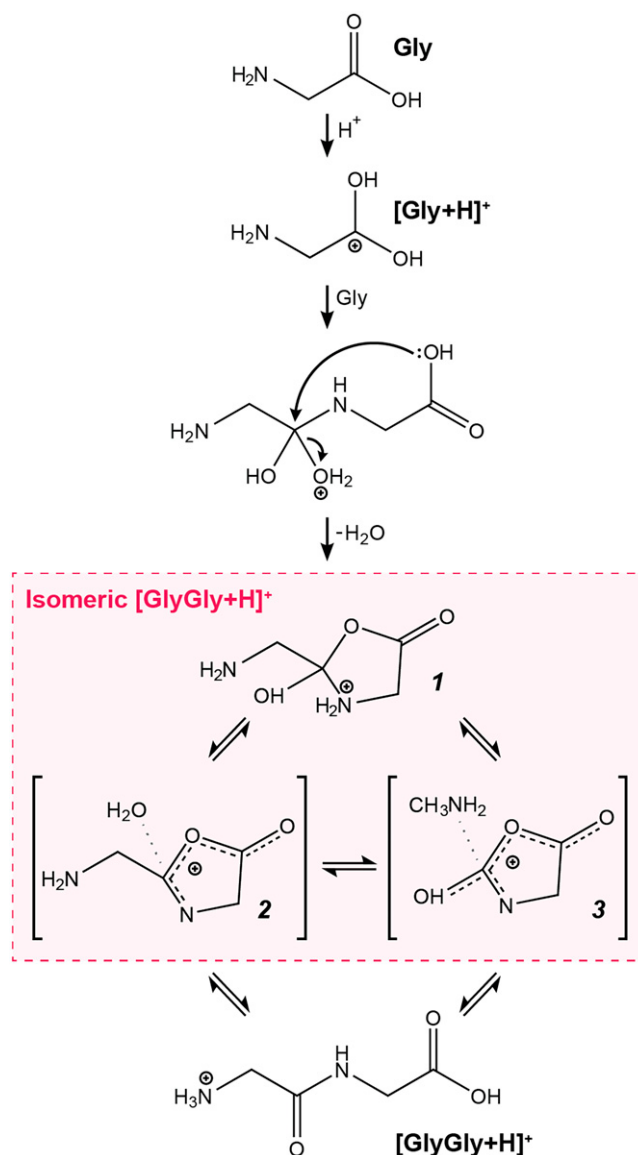
expected authentic form of the dipeptide, but if so, it then isomerizes, rapidly yielding the detected and more compact isomeric species, with both processes occurring at the droplet surface. The isomerization step of this proposed mechanism is consistent with a recent molecular dynamics study that found that particular metastable conformations of AlaAla are favored at the air–water interface due to greater intramolecular stabilization when the dipeptide is partially desolvated (80).

In an effort to determine a structure for the dipeptide isomers, several factors were considered based on the experimental findings which require 1) that the isomer have a more compact structure than the authentic dipeptide, 2) that there exists plausible interconversion pathways between the authentic and isomeric structures, 3) that the isomer structure be consistent with observed fragmentation profiles, and 4) that there be a favored route for chain extension to give higher order peptides from the isomer. Many attempts were carried out to deposit microdroplet-synthesized material for further characterization, although none were successful per NMR or Raman spectroscopic analysis of the collected product (*SI Appendix*, Table S2 for descriptions and discussion of collection experiments).

Based on our empirical observations and consideration of several plausible isomeric structures (*SI Appendix*, Table S3), we suggest that the microdroplet-synthesized isomeric dipeptides result from amino acid condensation with intramolecular cyclization to give 5-membered oxazolidinones. The resulting isomeric dipeptide ions exist as highly favorable ion-neutral complexes as well as fully covalent contributing forms (Scheme 1). Five-membered heterocycles, similar to the proposed structures, have been suggested as important prebiotic biomolecule precursors (81). The initial condensation reaction is likely driven by the extremely low interfacial pH of the microdroplet surface, as previously suggested for the condensation of *o*-phenyl diamines and carboxylic acids to form benzimidazoles and for the sequestration of carbon dioxide as the carbamic acids using free amines (41, 43, 82). Two ion-neutral complexes 2 and 3 (83, 84) are accessible from fully covalent oxazolidinone ion 1. The coexistence of covalent and ion-neutral forms of an ion has been implicated in gas-phase reactions of Gly (85), as well as the hydroxyl-amino exchange in protonated arginine (86), an isomerization process similar to that proposed here. These ion-neutral complexes are especially stable due to the high degree of electron delocalization (87) which covers almost the entire heterocycle.

The proposed oxazolidinone structures (ion-neutral complex and covalent forms, 1 to 3) (Scheme 1) satisfy all four of the criteria described above, whereas alternative possible structures of the isomeric dipeptide are inadequate (*SI Appendix*, Table S4). We suggest that the compact cyclic structures are favored at the air–water interface where compounds with larger dipole moments can be stabilized through alignment with the high surface electric field (79, 88), another factor that favors the oxazolidinone ions (*SI Appendix*, Table S5 and Fig. S13). This stabilizing effect can be further enhanced through favorable hydrogen bonding interactions in specific surface-aligned conformations (89, 90). Furthermore, the oxazolidinone ions provide an active carbonyl that is available for nucleophilic attack to yield authentic higher-order peptides upon ring opening (Fig. 5B). Such reactions in N-carboxy amino acid anhydrides, neutral analogs of the proposed species, readily form polypeptides in aqueous environments (91–94).

The findings presented here demonstrate the spontaneous generation of unique dipeptide species and authentic tri- through hexapeptides from free amino acids in pure aqueous microdroplets. It is noteworthy that these results also hold true



Scheme 1. Proposed mechanism for the microdroplet-mediated formation of $[\text{GlyGly}+\text{H}]^+$ dipeptide isomers that lead to authentic $[\text{GlyGly}+\text{H}]^+$ from free Gly. Protonation of free Gly on the carbonyl oxygen leads to condensation with a neutral Gly molecule followed by cyclization to oxazolidinone 1. This species has two ion-neutral complex forms where the neutral is either water (2) or methylamine (3).

in solutions of moderate salinity (*SI Appendix*, Fig. S14). We suggest that these condensation reactions are promoted by the distinctive dry environment of the air–water interface. Given the two-dimensional hydrogen bonding network experienced by compounds at the surface of aqueous microdroplets compared to the three-dimensional network in the interior, the air–water interface effectively serves as a low polarity drying surface, with its molecular structure influencing reactivity of surface-active species. Recent computations have argued a similar point by showing that water molecules at an air–water interface (2 to 3 molecular diameters) are characterized by an ice-like state, denoted by a distinctive molecular density gradient and perpendicular orientation at the interface (95). Further computational and spectroscopic results have highlighted the importance of both the number and orientation of hydrogen bonds on the surface activity of ions (96). Compounds oriented along O–H bonds perpendicular to the interface may experience a considerably greater electric field than those in the interior

of the droplet, providing enough energy to activate chemical bonds (79). Additionally, the difference in water content between the surface and the bulk of the droplet, together with the increased molecular order caused by the strong interfacial electric field, may induce alternative protonation sites (e.g., carbonyl vs. amine) due to partial solvation (97) and should facilitate dehydration reactions between surface-active compounds.

Interfacial chemistry appears to play a crucial role in facilitating biomolecule transformations in aqueous environments, as has been demonstrated in biphasic systems (91), cell condensates, and subcompartments (98), as well as in microdroplets (12, 13, 21, 29, 42, 51–53, 99, 100). The observed generation of peptides from free amino acids at the air–water interface of pure water droplets, the simplest of all prebiotic systems, suggests that settings such as atmospheric aerosols or sea spray may have provided a unique and ubiquitous environment to overcome the energetic hurdles associated with condensation and polymerization of biomolecules in water. Specifically, we suggest that the dry interface of aqueous microdroplets may be responsible for the dehydration required to form nucleosides, oligonucleotides, and polysaccharides, as well as peptides.

Materials and Methods

Chemicals. Liquid chromatography–MS–grade water (Fisher Scientific) was utilized for all experiments. Gly, GlyGly, Gly₃, Gly₄, Ala, and AlaAla (all with ≥99% purity) were purchased from Sigma-Aldrich. Ala₃ and Ala₄ were obtained from Toronto Research Chemicals. All reagents and solvents were used as received. The final concentration of all chemicals was 5 mM unless otherwise noted.

Microdroplet Formation and Ionization. nESI tips were made from borosilicate glass capillaries (Sutter Instrument Co.; outer diameter [O.D.] of 1.5 mm, inner diameter [I.D.] of 0.86 mm) pulled to ca. 5 μm O.D. using a Flaming/Brown micropipette puller (P-97, Sutter Instrument Co.). Solutions were ionized with ±2 kV spray potential supplied by the mass spectrometer to a platinum electrode placed inside the nESI capillary. The electrostatic spray ionization (ESSI) spray emitter was constructed using fused silica lines with 100-μm I.D. and 360-μm O.D. (PolyMicro), one tee assembly, one union assembly, two Nano-Tight sleeves, and a stainless-steel capillary (IDEX Health and Science). To maintain the flow of reagent solution at a rate of 10 μL/min, infuse syringe pumps (Standard Infusion PHD 22/2000, Harvard Apparatus) were utilized with gastight syringes (Hamilton Robotics). Nitrogen was used as the nebulizing gas at 180 psi. Voltage was supplied to the syringe needle during ESSI analysis with an external DC power supply (PMX110-0.6 A, Kikusui America, Inc.) at ±2 kV. nESI and ESSI emitters were all placed ~10 cm from the inlet of the mass spectrometer unless otherwise noted. To limit interfacial reactions, a droplet flight

distance of ~4 mm is often employed for routine analysis, whereas larger distances (such as those described in this work) are often used for microdroplet synthesis. Droplet fusion experiments were performed by placing two nESI capillaries and emitters ~10 cm away from the mass spectrometer and aligned at a ca. 65° angle to each other in a configuration that allowed their spray plumes to intersect prior to reaching the inlet.

MS and IMS. All low-resolution mass spectra and IT-CID product ion spectra were recorded using a LTQ XL ion trap mass spectrometer (Thermo Scientific). The parameters for the various ionization sources used are described above. HR mass measurements were acquired using a linear quadrupole ion trap coupled with an Orbitrap mass spectrometer (Thermo Scientific). In all cases, helium was used as bath gas. MS/MS control experiments were carried out using pure water to rule out chemical interferences on the fragmentation profiles observed.

IMS-MS experiments were performed using a Waters Synapt G2-Si quadrupole time-of-flight (ToF) mass spectrometer (Waters Corporation) equipped with a traveling wave IMS cell. A mass range of *m/z* 1 was selected using the quadrupole (LM resolution set to 18.5, HM resolution fixed at 15) prior to IMS analysis. IMS conditions were optimized to maximize resolution in the drift time separation. For the positive ion mode, the traveling wave velocity was selected as 1,500 m/s whereas the wave height was optimized to 40 V. For the negative ion mode, the wave velocity and wave height were set at 500 m/s and 25 V, respectively. In all cases, the IMS gas flow was kept at 90 mL/min. The scan time was set to 1 s, and data were acquired during 2 min for each sample. Additional parameters were not modified from the instrument default values. Experiments were performed using a nESI emitter with ±2 kV as the spray voltage (supplied by the instrument using a homebuilt connection). An extended DESI capillary was used as the heated inlet of the instrument, maintained at 250 °C for adequate ion transmission through the 90° bent capillary. Collisional cross-section calibration was performed using the Major Mix IMS/ToF calibration solution via the Intellistart assisted interface. For ion mobility experiments, the GlyGly was held constant at 10 μM (except in the case of the pure Gly control), while the concentration of Gly was varied up to 5 mM. IMS experiments used mixtures of 1:0, 1:125, 1:375, 1:500, and 0:1 GlyGly-Gly in pure water.

Data, Materials, and Software Availability. All study data are included in the article and/or *SI Appendix*.

ACKNOWLEDGMENTS. This work was supported by the NSF (Grant CHE-1905087), the Multi-University Research Initiative (MURI) of the Air Force Office of Scientific Research (FA9550-21-1-0170) via Stanford University (sub-award 62741613-204669), and Waters Corporation (Grant 40002775). D.T.H. acknowledges support from the National Science Foundation Graduate Research Fellowship (DGE-1842166). N.M.M. acknowledges support from the Eastman Summer Fellowship in Analytical Chemistry and the American Chemical Society Division of Analytical Chemistry Graduate Fellowship sponsored by Agilent Technologies.

1. H. J. Cleaves, Prebiotic chemistry: What we know, what we don't. *Evolution (N. Y.)* **5**, 342–360 (2012).
2. J. Dong, R. A. Fischer, L. P. Stixrude, C. R. Lithgow-Bertelloni, Constraining the volume of Earth's early oceans with a temperature-dependent mantle water storage capacity model. *AGU Adv.* **2**, 1–24 (2021).
3. M. J. Russell, A. J. Hall, A. J. Boyce, A. E. Fallick, 100th anniversary special paper: On hydrothermal convection systems and the emergence of life. *Econ. Geol.* **100**, 259–270 (2005).
4. F. Westall *et al.*, A hydrothermal-sedimentary context for the origin of life. *Astrobiology* **18**, 259–293 (2018).
5. E. Imai, H. Honda, K. Hatori, A. Brack, K. Matsuno, Elongation of oligopeptides in a simulated submarine hydrothermal system. *Science* **283**, 831–833 (1999).
6. R. Shapiro, Comments on 'concentration by evaporation and the prebiotic synthesis of cytosine'. *Orig. Life Evol. Biosph.* **32**, 275–278 (2002).
7. B. Damer, D. Deamer, The hot spring hypothesis for an origin of life. *Astrobiology* **20**, 429–452 (2020).
8. R. B. Hoover, "Comets, carbonaceous meteorites, and the origin of the biosphere" in *Biosphere Origin and Evolution*, N. Dobretsov, N. Kolchanov, A. Rozanov, G. Zavarzin (Springer, 2008), pp. 55–68.
9. A. S. Burton, J. C. Stern, J. E. Elsila, D. P. Glavin, J. P. Dworkin, Understanding prebiotic chemistry through the analysis of extraterrestrial amino acids and nucleobases in meteorites. *Chem. Soc. Rev.* **41**, 5459–5472 (2012).
10. R. I. Kaiser, A. M. Stockton, Y. S. Kim, E. C. Jensen, R. A. Mathies, On the formation of dipeptides in interstellar model ices. *Astrophys. J.* **765**, 111 (2013).
11. C. Menor-Salván, M. R. Marín-Yaseli, Prebiotic chemistry in eutectic solutions at the water-ice matrix. *Chem. Soc. Rev.* **41**, 5404–5415 (2012).
12. C. M. Dobson, G. B. Ellison, A. F. Tuck, V. Vaida, Atmospheric aerosols as prebiotic chemical reactors. *Proc. Natl. Acad. Sci. U.S.A.* **97**, 11864–11868 (2000).
13. H. Tervahattu, A. F. Tuck, V. Vaida, "Chemistry in prebiotic aerosols: A mechanism for the origin of life" in *Origins*, J. Seckbach (Springer Dordrecht, 2004), pp. 153–165.
14. A. Rimola, B. Civalleri, P. Ugliengo, Neutral vs zwitterionic glycine forms at the water/silica interface: Structure, energies, and vibrational features from B3LYP periodic simulations. *Langmuir* **24**, 14027–14034 (2008).
15. A. Rimola, M. Sodupe, P. Ugliengo, Role of mineral surfaces in prebiotic chemical evolution. In *Silico quantum mechanical studies*. *Life (Basel)* **9**, 10 (2019).
16. J. Bujdak, H. Slosiarikova, N. Texler, M. Schwendinger, B. M. Rode, On the possible role of montmorillonites in prebiotic peptide formation. *Monatsh. Chem.* **125**, 1033–1039 (1994).
17. J. F. Lambert, M. Jaber, T. Georgelin, L. Stievano, A comparative study of the catalysis of peptide bond formation by oxide surfaces. *Phys. Chem. Chem. Phys.* **15**, 13371–13380 (2013).
18. V. Erastova, M. T. Degiacomi, D. G. Fraser, H. C. Greenwell, Mineral surface chemistry control for origin of prebiotic peptides. *Nat. Commun.* **8**, 20333 (2017).
19. N. Lahav, D. White, S. Chang, Peptide formation in the prebiotic era: Thermal condensation of glycine in fluctuating clay environments. *Science* **201**, 67–69 (1978).
20. D. G. Fraser, D. Fitz, T. Jakschitz, B. M. Rode, Selective adsorption and chiral amplification of amino acids in vermiculite clay-implications for the origin of biochirality. *Phys. Chem. Chem. Phys.* **13**, 831–838 (2011).
21. A. M. Deal, R. J. Rapf, V. Vaida, Water-air interfaces as environments to address the water paradox in prebiotic chemistry: A physical chemistry perspective. *J. Phys. Chem. A* **125**, 4929–4942 (2021).
22. W. M. McGee, S. A. McLuckey, Efficient and directed peptide bond formation in the gas phase via ion/ion reactions. *Proc. Natl. Acad. Sci. U.S.A.* **111**, 1288–1292 (2014).

23. H. Wincel, R. H. Fokkens, N. M. M. Nibbering, Peptide bond formation in gas-phase ion/molecule reactions of amino acids: A novel proposal for the synthesis of prebiotic oligopeptides. *Rapid Commun. Mass Spectrom.* **14**, 135–140 (2000).
24. J. H. Jensen, K. K. Baldridge, M. S. Gordon, Uncatalyzed peptide bond formation in the gas phase. *J. Phys. Chem.* **96**, 8340–8351 (1992).
25. A. G. Gale, T. T. Odbadrakh, B. T. Ball, G. C. Shields, Water-mediated peptide bond formation in the gas phase: A model prebiotic reaction. *J. Phys. Chem. A* **124**, 4150–4159 (2020).
26. T. D. Campbell *et al.*, Prebiotic condensation through wet-dry cycling regulated by deliquescence. *Nat. Commun.* **10**, 4508 (2019).
27. J. N. Ervin, M. Bouza, F. M. Fernández, J. G. Forsythe, Proline behavior in model prebiotic peptides formed by wet-dry cycling. *ACS Earth Space Chem.* **4**, 1349–1359 (2020).
28. J. K. Kumar, J. S. Oliver, Proximity effects in monolayer films: Kinetic analysis of amide bond formation at the air-water interface using ¹H NMR spectroscopy. *J. Am. Chem. Soc.* **124**, 11307–11314 (2002).
29. E. C. Griffith, V. Vaida, In situ observation of peptide bond formation at the water-air interface. *Proc. Natl. Acad. Sci. U.S.A.* **109**, 15697–15701 (2012).
30. Z. Wei *et al.*, High yield accelerated reactions in nonvolatile microthin films: Chemical derivatization for analysis of single-cell intracellular fluid. *Chem. Sci. (Camb.)* **9**, 7779–7786 (2018).
31. H. Nie *et al.*, High-yield gram-scale organic synthesis using accelerated microdroplet/thin film reactions with solvent recycling. *Chem. Sci. (Camb.)* **11**, 2356–2361 (2020).
32. R. M. Bain, C. J. Pulliam, F. They, R. G. Cooks, Accelerated chemical reactions and organic synthesis in Leidenfrost droplets. *Angew. Chem. Int. Ed. Engl.* **55**, 10478–10482 (2016).
33. Y. Li *et al.*, Accelerated forced degradation of pharmaceuticals in levitated microdroplet reactors. *Chemistry* **24**, 7349–7353 (2018).
34. Y. Li, T. F. Mehari, Z. Wei, Y. Liu, R. G. Cooks, Reaction acceleration at air-solution interfaces: Anisotropic rate constants for Katritzky transamination. *J. Mass Spectrom.* **56**, e4585 (2021).
35. P. W. Fedick *et al.*, Screening of the Suzuki cross-coupling reaction using desorption electrospray ionization in high-throughput and in Leidenfrost droplet experiments. *J. Am. Soc. Mass Spectrom.* **30**, 2144–2151 (2019).
36. H. M. Brown, K. R. Doppalapudi, P. W. Fedick, Accelerated synthesis of energetic precursor cage compounds using confined volume systems. *Sci. Rep.* **11**, 24093 (2021).
37. J. K. Lee, H. G. Nam, R. N. Zare, Microdroplet fusion mass spectrometry: Accelerated kinetics of acid-induced chlorophyll demetallation. *Q. Rev. Biophys.* **50**, e2 (2017).
38. N. Narendra *et al.*, Quantum mechanical modeling of reaction rate acceleration in microdroplets. *J. Phys. Chem. A* **124**, 4984–4989 (2020).
39. B. M. Marsh, K. Iyer, R. G. Cooks, Reaction acceleration in electrospray droplets: Size, distance, and surfactant effects. *J. Am. Soc. Mass Spectrom.* **30**, 2022–2030 (2019).
40. H. Chen, L. S. Eberlin, M. Neffiu, R. Augusti, R. G. Cooks, Organic reactions of ionic intermediates promoted by atmospheric-pressure thermal activation. *Angew. Chem. Int. Ed. Engl.* **47**, 3422–3425 (2008).
41. P. Basuri, L. E. Gonzalez, N. M. Morato, T. Pradeep, R. G. Cooks, Accelerated microdroplet synthesis of benzimidazoles by nucleophilic addition to protonated carboxylic acids. *Chem. Sci. (Camb.)* **11**, 12686–12694 (2020).
42. P. Basuri, J. S. Kumar, S. Das, T. Pradeep, Accelerated non-enzymatic fatty acid esterification during microdroplet collision: A method for enhanced sustainability. *ACS Sustain. Chem. & Eng.* **2022**, 8587 (2022).
43. K. H. Huang, Z. Wei, R. G. Cooks, Accelerated reactions of amines with carbon dioxide driven by superacid at the microdroplet interface. *Chem. Sci. (Camb.)* **12**, 2242–2250 (2020).
44. L. Qiu, M. D. Pismos, R. G. Cooks, Spontaneous oxidation of aromatic sulfones to sulfonic acids in microdroplets. *J. Am. Soc. Mass Spectrom.* **33**, 1362–1367 (2022).
45. L. Qiu, N. M. Morato, K. H. Huang, R. G. Cooks, Spontaneous water radical cation oxidation at double bonds in microdroplets. *Front Chem.* **10**, 903774 (2022).
46. S. Banerjee, R. N. Zare, Syntheses of isoquinoline and substituted quinolines in charged microdroplets. *Angew. Chem. Int. Ed. Engl.* **54**, 14795–14799 (2015).
47. Z. Wei, Y. Li, R. G. Cooks, X. Yan, Accelerated reaction kinetics in microdroplets: Overview and recent developments. *Annu. Rev. Phys. Chem.* **71**, 31–51 (2020).
48. L. Qiu, Z. Wei, H. Nie, R. G. Cooks, Reaction acceleration promoted by partial solvation at the gas/solution interface. *ChemPlusChem* **86**, 1362–1365 (2021).
49. W. Wang *et al.*, Water microdroplets allow spontaneously abiotic production of peptides. *J. Phys. Chem. Lett.* **12**, 5774–5780 (2021).
50. A. W. Schwartz, "Origins of the RNA world" in *The Molecular Origins of Life: Assembling Pieces of the Puzzle* (ed. A. Brack) Cambridge University Press, New York, (2010), pp. 237–254.
51. I. Nam, J. K. Lee, H. G. Nam, R. N. Zare, Abiotic production of sugar phosphates and uridine ribonucleoside in aqueous microdroplets. *Proc. Natl. Acad. Sci. U.S.A.* **114**, 12396–12400 (2017).
52. I. Nam, H. G. Nam, R. N. Zare, Abiotic synthesis of purine and pyrimidine ribonucleosides in aqueous microdroplets. *Proc. Natl. Acad. Sci. U.S.A.* **115**, 36–40 (2018).
53. V. Vaida, Prebiotic phosphorylation enabled by microdroplets. *Proc. Natl. Acad. Sci. U.S.A.* **114**, 12359–12361 (2017).
54. L. M. Barge, E. Flores, M. M. Baum, D. G. VanderVelde, M. J. Russell, Redox and pH gradients drive amino acid synthesis in iron oxyhydroxide mineral systems. *Proc. Natl. Acad. Sci. U.S.A.* **116**, 4828–4833 (2019).
55. J. K. Lee, D. Samanta, H. G. Nam, R. N. Zare, Micrometer-sized water droplets induce spontaneous reduction. *J. Am. Chem. Soc.* **141**, 10585–10589 (2019).
56. J. E. Biegajski, D. A. Cadenehead, P. N. Prasad, Interfacial polymerization of monomolecular and Langmuir-Blodgett films of ((butoxycarbonyl)methyl)urethane diacetylenes. *Macromolecules* **24**, 298–303 (1991).
57. X. Yan, R. M. Bain, R. G. Cooks, Organic reactions in microdroplets: Reaction acceleration revealed by mass spectrometry. *Angew. Chem. Int. Ed. Engl.* **55**, 12960–12972 (2016).
58. S. Vaitheeswaran, D. Thirumalai, Hydrophobic and ionic interactions in nanosized water droplets. *J. Am. Chem. Soc.* **128**, 13490–13496 (2006).
59. J. K. Lee, D. Samanta, H. G. Nam, R. N. Zare, Spontaneous formation of gold nanostructures in aqueous microdroplets. *Nat. Commun.* **9**, 1562 (2018).
60. J. K. Lee *et al.*, Spontaneous generation of hydrogen peroxide from aqueous microdroplets. *Proc. Natl. Acad. Sci. U.S.A.* **116**, 19294–19298 (2019).
61. D. Gao, F. Jin, J. K. Lee, R. N. Zare, Aqueous microdroplets containing only ketones or aldehydes undergo Dakin and Baeyer-Villiger reactions. *Chem. Sci. (Camb.)* **10**, 10974–10978 (2019).
62. A. Bouillant *et al.*, Leidenfrost wheels. *Nat. Phys.* **14**, 1188–1192 (2018).
63. A. Fallah-Araghi *et al.*, Enhanced chemical synthesis at soft interfaces: A universal reaction-adsorption mechanism in microcompartments. *Phys. Rev. Lett.* **112**, 028301 (2014).
64. D. N. Mortensen, E. R. Williams, Theta-glass capillaries in electrospray ionization: Rapid mixing and short droplet lifetimes. *Anal. Chem.* **86**, 9315–9321 (2014).
65. Z. Zhou, X. Yan, Y.-H. Lai, R. N. Zare, Fluorescence polarization anisotropy in microdroplets. *J. Phys. Chem. Lett.* **9**, 2928–2932 (2018).
66. M. Girod, E. Moyano, D. I. Campbell, R. G. Cooks, Accelerated bimolecular reactions in microdroplets studied by desorption electrospray ionization mass spectrometry. *Chem. Sci. (Camb.)* **2**, 501–510 (2011).
67. K. Luo *et al.*, Reaction of chloroauric acid with histidine in microdroplets yields a catalytic Au(His)₂ complex. *Chem. Sci. (Camb.)* **11**, 2558–2565 (2020).
68. N. Sahota *et al.*, A microdroplet-accelerated Biginelli reaction: Mechanisms and separation of isomers using IMS-MS. *Chem. Sci. (Camb.)* **10**, 4822–4827 (2019).
69. M. F. Ruiz-Lopez, J. S. Francisco, M. T. C. Martins-Costa, J. M. Anglada, Molecular reactions at aqueous interfaces. *Nat. Rev. Chem.* **4**, 459–475 (2020).
70. Y. Ju *et al.*, Aqueous-microdroplet-driven abiotic synthesis of ribonucleotides. *J. Phys. Chem. Lett.* **13**, 567–573 (2022).
71. A. F. Tuck, Gibbs free energy and reaction rate acceleration in and on microdroplets. *Entropy (Basel)* **21**, 1044 (2019).
72. J. K. Lee, S. Banerjee, H. G. Nam, R. N. Zare, Acceleration of reaction in charged microdroplets. *Q. Rev. Biophys.* **48**, 437–444 (2015).
73. D. S. Wishart *et al.*, HMDB 5.0: The Human Metabolome Database for 2022. *Nucleic Acids Res.* **50**, D622–D631N (2022).
74. P. B. Armentrout, Mass spectrometry—Not just a structural tool: The use of guided ion beam tandem mass spectrometry to determine thermochemistry. *J. Am. Soc. Mass Spectrom.* **13**, 419–434 (2002).
75. K. J. Hart, S. A. McLuckey, G. L. Glish, Evidence of isomerization during ion isolation in the quadrupole ion trap. *J. Am. Soc. Mass Spectrom.* **3**, 680–682 (1992).
76. V. H. Wysocki, H. I. Kenttämaa, Collisional activation of distonic radical cations and their conventional isomers in quadrupole tandem mass spectrometry. *J. Am. Chem. Soc.* **112**, 5110–5116 (1990).
77. H. I. Kenttämaa, Effects of stepwise excitation on fragmentation of gas phase ions: An especially striking case. *Org. Mass Spectrom.* **20**, 703–714 (1985).
78. J. K. Lee, S. Kim, H. G. Nam, R. N. Zare, Microdroplet fusion mass spectrometry for fast reaction kinetics. *Proc. Natl. Acad. Sci. U.S.A.* **112**, 3898–3903 (2015).
79. H. Hao, I. Leven, T. Head-Gordon, Can electric fields drive chemistry for an aqueous microdroplet? *Nat. Commun.* **13**, 280 (2022).
80. A. N. Singh, D. T. Limmer, Peptide isomerization is suppressed at the air-water interface. *J. Phys. Chem. Lett.* **13**, 574–579 (2022).
81. C. A. Cole, N. J. Demarais, Z. Yang, T. P. Snow, V. M. Bierbaum, Heterocyclic anions of astrobiological interest. *Astrophys. J.* **779**, 181 (2013).
82. L. Feng *et al.*, Ammonium bicarbonate significantly accelerates the microdroplet reactions of amines with carbon dioxide. *Anal. Chem.* **93**, 15775–15784 (2021).
83. R. D. Bowen, The role of ion-neutral complexes in the reactions of onium ions and related species. *Org. Mass Spectrom.* **28**, 1577–1595 (1993).
84. R. D. Bowen, Ion-neutral complexes. *Acc. Chem. Res.* **24**, 364–371 (1991).
85. R. A. J. O'Hair, M. A. Freitas, T. D. Williams, Gas phase reactions of the cyclic ethylenealonium ions (CH₂)₂X⁺ (X = Cl, Br) with glycine. *J. Org. Chem.* **61**, 2374–2382 (1996).
86. T. Cai *et al.*, Gas-phase intramolecular hydroxyl-amino exchange of protonated arginine and verified by the synthetic intermediate compound. *J. Mass Spectrom.* **53**, 700–704 (2018).
87. R. D. Bowen, W. H. C. Martin, C. E. Hudson, D. J. McAdoo, Experimental and computational evidence for C=O π-bonding in [CH₂OH]⁺ and related oxonium ions. *Eur J Mass Spectrom (Chichester)* **26**, 187–194 (2020).
88. H. Xiong, J. K. Lee, R. N. Zare, W. Min, Strong electric field observed at the interface of aqueous microdroplets. *J. Phys. Chem. Lett.* **11**, 7423–7428 (2020).
89. R. D. Hoehn *et al.*, Hydrogen bonding and orientation effects on the accommodation of methylamine at the air-water interface. *J. Chem. Phys.* **144**, 214701 (2016).
90. C. Zhu, X. C. Zeng, J. S. Francisco, I. Gladich, Hydration, solvation, and isomerization of methylglyoxal at the air/water interface: New mechanistic pathways. *J. Am. Chem. Soc.* **142**, 5574–5582 (2020).
91. Z. Song *et al.*, Synthesis of polypeptides via bioinspired polymerization of in situ purified N-carboxyanhydrides. *Proc. Natl. Acad. Sci. U.S.A.* **116**, 10658–10663 (2019).
92. H. R. Kricheldorf, Polypeptides and 100 years of chemistry of α-amino acid N-carboxyanhydrides. *Angew. Chem. Int. Ed. Engl.* **45**, 5752–5784 (2006).
93. C. Fetsch, A. Grossmann, L. Holz, J. F. Nawroth, R. Luxenhofer, Polypeptides from n-substituted glycine n-carboxyanhydrides: Hydrophilic, hydrophobic, and amphiphilic polymers with poisson distribution. *Macromolecules* **44**, 6746–6758 (2011).
94. J. Cheng, T. J. Deming, Synthesis of polypeptides by ring-opening polymerization of α-amino acid N-carboxyanhydrides. *Top. Curr. Chem.* **310**, 1–26 (2012).
95. N. L. Odendahl, P. L. Geissler, Local ice-like structure at the liquid water surface. *J. Am. Chem. Soc.* **144**, 11178–11188 (2022).
96. T. M. Chang, R. J. Cooper, E. R. Williams, Locating protonated amines in clathrates. *J. Am. Chem. Soc.* **135**, 14821–14830 (2013).
97. T. M. Chang, J. S. Prell, E. R. Warrick, E. R. Williams, Where's the charge? Protonation sites in gaseous ions change with hydration. *J. Am. Chem. Soc.* **134**, 15805–15813 (2012).
98. W. Stroberg, S. Schnell, Do cellular condensates accelerate biochemical reactions? Lessons from microdroplet chemistry. *Biophys. J.* **115**, 3–8 (2018).
99. X. Zhong, H. Chen, R. N. Zare, Ultrafast enzymatic digestion of proteins by microdroplet mass spectrometry. *Nat. Commun.* **11**, 1049 (2020).
100. X. Zhong, H. Chen, R. N. Zare, Ultrafast enzymatic digestion of deoxyribonucleic acid in aqueous microdroplets for sequence discrimination and identification. *QRB Discov.* **2**, e4 (2021).